Prediction of Compressible, Laminar Viscous Flows Using a Time-Marching Control Volume and Multiple-Grid Technique

Roger L. Davis* and Ron Ho Ni†
United Technologies Corporation, East Hartford, Connecticut
and
Wallace W. Bowley‡
University of Connecticut, Storrs, Connecticut

A new numerical technique for the prediction of laminar flows through the solution of the time-dependent Navier-Stokes equations is presented. The solution procedure consists of an explicit, time-marching, control volume technique which is second-order accurate in time and space. This scheme has been combined with a multiple-grid convergence acceleration technique to form an efficient viscous flow solver. The technique has been applied to a variety of internal and external geometries to obtain steady-state viscous solutions. Sample cases comparing the numerical results to experimental data are shown to demonstrate the accuracy and efficiency of the technique.

Nomenclature

A = area of element
c = speed of sound
C_P = specific heat at constant pressure
h = static enthalpy
H = total enthalpy
M = Mach number
N = number of corner nodes of element
p = pressure
R = gas constant (air)
T = temperature
t = time
u = nondimensionalized axial (x) component of velocity
v = nondimensionalized tangential (y) component of velocity
V = velocity
x = axial component of Cartesian coordinate system
y = tangential component of Cartesian coordinate system
Δ = increment
μ = coefficient of viscosity
ρ = nondimensionalized density
ϕ = arbitrary primary variable

Subscripts and Superscripts

e = element
i = node
T = stagnation conditions
x = axial component
y = tangential component
1 = upstream condition
2 = downstream condition
$( )^*$ = transpose of matrix

Presented as Paper 83-1896 at the AIAA Sixth Computational Fluid Dynamics Conference, Danvers, Mass., received Aug. 3, 1983; revision received Jan. 30, 1984.

*Research Engineer, United Technologies Research Center. Member AIAA.
†Senior Research Engineer, Pratt & Whitney Aircraft. Member AIAA.
‡Professor, Mechanical Engineering. Member AIAA.

Introduction

At the onset of developing a viscous flow solver for general engineering applications, the types of flowfields to be predicted, as well as accuracy, flexibility, and speed or computational efficiency of the numerical technique to be used, must be considered carefully. A viscous solver which can predict flows over a wide range of compressibility conditions from subsonic through supersonic speeds, including shocked flows, is usually desired. In addition, flows with vorticies such as found in secondary, wake, or separated flows should be modeled in such a procedure. Time-marching schemes in conjunction with the Navier-Stokes equations take into account most of the above considerations, but usually lack in computational efficiency. Due to the large number of grid points needed to resolve viscous flows, the resulting calculation times involved in reaching a steady-state solution using these schemes is usually quite large. There are ways of reducing these computational times, however. An artificial method is to take advantage of a powerful computer. Spradley et al.[1] have developed a time-marching, explicit, control volume technique for laminar flows using a MacCormack-like scheme.[2] Computational times for this code are kept at reasonable levels through the use of a vector processor. A more effective way of reducing computational times for time-marching schemes is to make the numerical method itself more efficient. New techniques have been developed recently which accelerate convergence of time-marching routines. An approach developed by MacCormack[3] modifies the changes of primary variables in each stage of the original predictor-corrector explicit technique using an implicit-like correction step which has the effect of propagating local changes through the entire global domain. Ni[4] has developed a procedure which combines a new second-order scheme with a multiple-grid algorithm to solve the Euler equations. The multiple-grid scheme used in this code is a very effective explicit acceleration technique for hyperbolic equations. The results of the multiple-grid scheme are similar to the correction step of the MacCormack technique in that local changes are propagated through the global domain at a high speed. Johnson[5] has used the Ni multiple-grid algorithm to enhance the convergence of an explicit MacCormack predictor-corrector scheme[2] for the calculation of inviscid and viscous flows. Recent research[6] has led to the development of a second-order accurate, laminar time-marching

solver which when combined with the Ni multiple-grid scheme provides for an efficient means of calculating a wide range of viscous flows. Unlike the technique developed by Johnson, an integral Lax-Wendroff-type scheme is used for the fine grid solution in this work. As a consequence, the multiple-grid algorithm becomes tightly coupled and consistent with the fine grid solver.

The technique described in this paper is an explicit, time-marching, control volume scheme. Laminar shear stress terms, appropriate time step, and boundary condition requirements properly account for the calculation of laminar viscous flows. The integration of the controlling equations is performed using finite element techniques which are known for their accuracy and flexibility in describing the shape of the element as well as the primary variable functions s ithin the element. Instead of minimizing a variational or error function, as performed in a true finite element approach, basis functions used to define the variation of the primary variables within discrete elements are substituted into the Navier-Stokes equations directly, and, upon integration, yield a two-step, finite element, control volume technique. As a subset of the finite element scheme, a projected area control volume integration technique arises when bilinear elements and linear primary variable functions within the elements are used. Some accuracy of the element integrations may be lost due to the linear approximations in this scheme, but the ability to reduce the two-step technique into a one-step scheme arises yielding a more efficient routine.

The Ni multiple-grid convergence acceleration routine used in conjunction with this numerical technique calculates second-order time-rate changes over successively larger grids resulting in a propagation of a local time-rate changes through the global domain with relatively few operations. Convergence to a steady-state viscous solution is reached in significantly fewer time steps with the use of this routine. The multiple-grid acceleration routine demonstrates the most computational time savings when combined with the control volume one-step scheme since it is the more efficient of the two numerical techniques.

The multiple-grid convergence acceleration scheme has not yet been connected to the finite element two-step solver due to a lack of time. Application should be straightforward, however, since the numerics involved in the multiple-grid accelerator are quite similar to those of the Lax-Wendroff technique used in the fine grid solver. Without the multiple-grid accelerator, the computational times for the three-dimensional finite element solver become quite large. Some three-dimensional viscous flows have been calculated, however, with encouraging results. These results will be addressed only briefly at this time, though. A three-dimensional control volume viscous solver does not exist at this time. Therefore, for the sake of continuity and brevity, the theory for two-dimensional laminar viscous flows will be discussed only within this paper. The extension to three-dimensional flows is relatively straightforward.

Navier-Stokes Equations

The differential Navier-Stokes equations prescribe the conservation of mass, momentum, and energy of the fluid. The equation of state and the viscosity law relate the pressure and shear stresses to the density and temperature. Additional assumptions of a perfect gas and adiabatic flow aid in simplifying the set of equations to be solved. For adiabatic flow with unit Prandtl number, the differential energy equation reduces to an algebraic equation relating the stagnation and static temperature.

The two-dimensional Navier-Stokes equations in conservation form are

$$\frac{\partial U}{\partial t}+\frac{\partial E}{\partial x}+\frac{\partial F}{\partial y}=0 \tag{1}$$

where

$$U=\begin{bmatrix}\rho\\ \rho u\\ \rho v\end{bmatrix}\quad E=\begin{bmatrix}\rho u\\ \rho u^2+p-\tau_{xx}\\ \rho uv-\tau_{xy}\end{bmatrix}\quad F=\begin{bmatrix}\rho v\\ \rho uv-\tau_{xy}\\ \rho v^2+p-\tau_{yy}\end{bmatrix} \tag{2}$$

and

$$\tau_{xx}=\mu\left[\frac{4}{3}\frac{\partial u}{\partial x}-\frac{2}{3}\frac{\partial v}{\partial y}\right]\qquad \tau_{yy}=\mu\left[\frac{4}{3}\frac{\partial v}{\partial y}-\frac{2}{3}\frac{\partial u}{\partial x}\right]$$

$$\tau_{xy}=\mu\left[\frac{\partial u}{\partial y}+\frac{\partial v}{\partial x}\right] \tag{3}$$

The energy equation is given by

$$H=h+(V^2/2) \tag{4}$$

For a perfect gas,

$$p=\rho RT,\quad H=C_PT_T,\quad C_P=\gamma R/(\gamma-1)$$

$$c^2=\gamma RT,\quad h=C_PT \tag{5}$$

Sutherland's law is used to relate the coefficient of viscosity to the static temperature for air,

$$\frac{\mu}{\mu_\infty}=\left(\frac{T}{T_\infty}\right)^{3/2}\frac{T_\infty+198.6^\circ\mathrm{R}}{T+198.6^\circ\mathrm{R}}\quad\text{(viscous)}$$

$$\mu=0.0\quad\text{(inviscid)} \tag{6}$$

The velocity components are nondimensionalized by the upstream total velocity and the density is nondimensionalized by the upstream density.

Computational Mesh

A general flowfield may be broken into small regular polygons. These polygons are quadrilaterals for two-dimensional flows. The computational mesh may be defined through conformal mapping techniques, body-fitting schemes, or simple algebraic algorithms. The meshes used in the calculations herein are all body fitted and are generated completely independent of the flow solver.

Finite Element Two-Step Numerical Technique

The finite element two-step technique consists of calculating the first-order change in time of the primary variables, ρ, u, and v, by integrating Eqs. (1-3). A distribution of $1/N$, where N is the number of corner nodes making up a polygon, of the first-order time-rate change is given to each corner node of the polygonal element. Second-order changes in time are calculated by taking time derivatives of the Navier-Stokes equations and then integrating them over new spatially translated control volumes defined by connecting the centroids of adjacent primary elements. The time step for this explicit solver is based on the Courant, Friedricks, and Lewy (CFL) wave propagation and diffusion stability criteria.[7] The procedure of updating the primary variables in time is performed according to a second-order accurate Taylor series expansion in time

$$\phi^{t+\Delta t}=\phi^t+\underbrace{\frac{\partial\phi}{\partial t}\,\Delta t}_{\substack{\text{First-}\\ \text{order}\\ \text{change}}}+\underbrace{\frac{\partial^2\phi}{\partial t^2}\,\frac{\Delta t^2}{2}}_{\substack{\text{Second-}\\ \text{order}\\ \text{change}}} \tag{7}$$

where $\phi=\rho$, u, and v.

First-Order Changes in Time

Let each of the primary variables and the velocity component spatial derivatives within a control volume be represented by the function

$$\phi_e = A_1 + A_2 x + A_3 y = [A_1 A_2 A_3] \begin{bmatrix} 1 \\ x \\ y \end{bmatrix} = [A]^*[SF] \tag{8}$$

Quadratic variable functions have also been used in this scheme.[6]

The polygonal element may be triangularized as shown in Fig. 1a to produce subvolumes which have the correct number of nodes to allow for the finite element approximation. By substituting the nodal locations of the subvolumes into the matrix $[SF]$, solving for the coefficient matrix $[A]$, and substituting back into Eq. (8), the variable function arises in the form:

$$\phi_e = [SF]^*[K][\phi_i] \tag{9}$$

where $[K]$ is the stiffness matrix which contains the geometric weights of the subvolume nodes.

Equation (9) represents the finite element shape function for each of the primary variables and the velocity component spatial derivatives. Substitution of this function into the Navier-Stokes equations (1-3) directly, instead of an error function derived from these equations, results in a control volume scheme upon integration. Thus, the finite element control volume technique developed can utilize a wide range of basis functions to describe the variation of the primary variables within the discrete elements for increased accuracy, while maintaining the simplicity of a control volume approach. The discrete equations for the first-order change in time of the primary variables resulting from the integration of Eqs. (1-3) and the use of Eq. (9) is given in Appendix A. Green's theorem is used to convert area integrals for two-dimensional geometries into closed line integrals.

Standard second-order accurate finite difference formulas based upon adjacent nodal values are used to calculate the grid-wise velocity derivatives at each node for all shear stress terms. Metrics are then used to transform the grid-wise derivatives into spatial derivatives. For instance, consider the calculation of the derivatives $\partial u/\partial x$ and $\partial u/\partial y$ on a two-dimensional mesh system, as shown in Fig. 2.

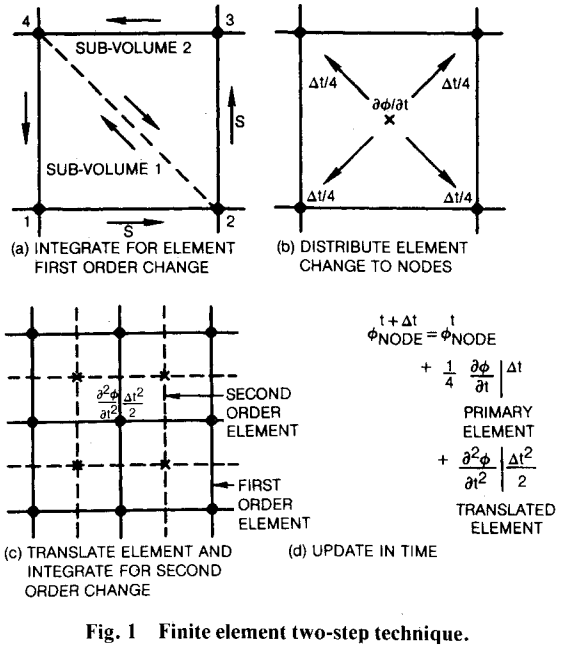

Fig. 1 Finite element two-step technique.

The value of $\partial u/\partial x$ may be calculated using

$$\frac{\partial u}{\partial M} = \nabla u \cdot M \tag{10}$$

where M is either the I or J grid tangent vectors which lie along the streamwise and transverse grid lines, respectively. The values of $\partial u/\partial x$ and $\partial u/\partial y$ may be calculated in terms of $\partial u/\partial I$ and $\partial u/\partial J$ from Eq. (10) resulting in

$$\frac{\partial u}{\partial x} = \frac{1}{(I_x J_y - I_y J_x)}\left[J_y \frac{\partial u}{\partial I} - I_y \frac{\partial u}{\partial J}\right]$$

$$\frac{\partial u}{\partial y} = \frac{1}{(I_x J_y - I_y J_x)}\left[I_x \frac{\partial u}{\partial J} - J_x \frac{\partial u}{\partial I}\right] \tag{11}$$

where subscripts x and y refer to the x and y components of the vectors. The derivative $\partial u/\partial I$ is calculated using a second-order accurate central difference formula (except at solid boundaries where forward or backward differencing is used) which for uniform meshes reduces to

$$\frac{\partial u}{\partial I} = \frac{u_{i+1} - u_{i-1}}{I_{i+1} - I_{i-1}} \tag{12}$$

and the components of I are simply

$$I_x = \frac{x_{i+1} - x_{i-1}}{I_{i+1} - I_{i-1}} \qquad I_y = \frac{y_{i+1} - y_{i-1}}{I_{i+1} - I_{i-1}} \tag{13}$$

The effect of using this technique is that the finite difference formulas used to calculate derivatives such as $\partial u/\partial x$ rotate correctly as the mesh changes directions.

Equations (A1-A3) in Appendix A give the first-order change of ρ, ρu, and ρv with respect to the time of the subvolume. By assembling the matrices of the subvolumes into matrices for the polygons prior to calculation of any time-rate changes, the first-order change in time of the primary variables within the polygons may be calculated directly using

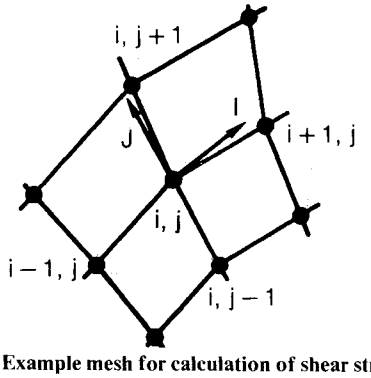

Fig. 2 Example mesh for calculation of shear stresses.

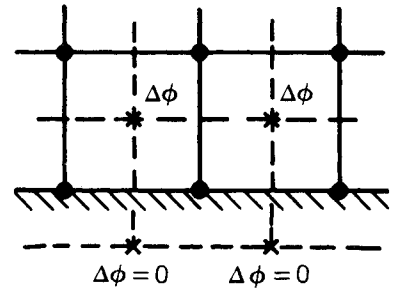

Fig. 3 Imaginary boundary nodes.

these same equations. The integral matrices of Eq. (A4) then become assembled matrices for the polygons. The calculation of the time-rate changes, therefore, are performed by a series of simple matrix multiplication steps. The first-order changes of the velocity components then are calculated from the chain rule.

The first-order change at the polygonal element corner nodes is calculated through a distribution of $1/N$ of the element change to each corner node, as shown in Fig. 1b. This distribution step produces a second-order accurate solution at each corner node.

Time Step

The time step Δt is calculated according to the CFL and diffusion stability criteria which are described by Richtmyer and Morton[8]:

$$\Delta t \leq \min\left[\frac{|L|}{|V\cdot L|+c+(2\mu/|L|)}\right] \tag{14}$$

where L is the directional vector crossing the element in the streamwise and transverse mesh directions. The time step is calculated for each polygonal element.

Second-Order Changes in Time

Second-order changes in time of the primary variables are calculated by integrating the time derivative of the Navier-Stokes equations over the local domain of a new spatially translated element. The second-order element consists of that area inside the perimeter which connects the centroids of the primary polygonal elements, as shown in Fig. 1c.

As was the case for the first-order change, each of the primary variables, as well as their spatial and time-rate derivatives, are represented by finite element functions as given by Eq. (9). Substitution of these functions into the time derivative of the Navier-Stokes equations and subsequent integration yields the finite element equations for the second-order changes in time. These finite element discretized equations may be obtained by taking the time-rate derivative of the first-order change finite element equations (A1-A3) in Appendix A. The second-order time-rate changes are applied directly to the primary element corner node located at or near the center of the translated second-order element (see Fig. 1c). Second-order time-rate changes in the velocity components are calculated from the second-order flux changes using the chain rule.

When necessary, the spatial derivatives of the unsteady shear stress terms associated with the time derivative fo the Navier-Stokes equations are calculated with second-order accurate difference formulas using time-rate velocity changes of adjacent first-order elements. These unsteady viscous terms have been found, however, to be necessary only for stability in cases where strong channel wall curvature or shocks exist. The accuracy of the steady-state Navier-Stokes solution does not depend on their existence.

Boundary Conditions

Boundary conditions may be divided into two types: freestream and solid walls. The freestream boundary condition takes the form of either a constant total pressure, static pressure, or "radiation" condition to be defined below. Either a constant static or total pressure condition is used for the upstream freestream boundary, depending on the geometry of the problem. For viscous channel flow, a constant static pressure condition is imposed. For inviscid channel flow and general external flows, a constant total pressure condition is more suitable. The downstream freestream condition consists of constant static pressure for subsonic channel flow or a radiation condition for supersonic channel flow and general external flows. The radiation condition is performed through a simple updating of the

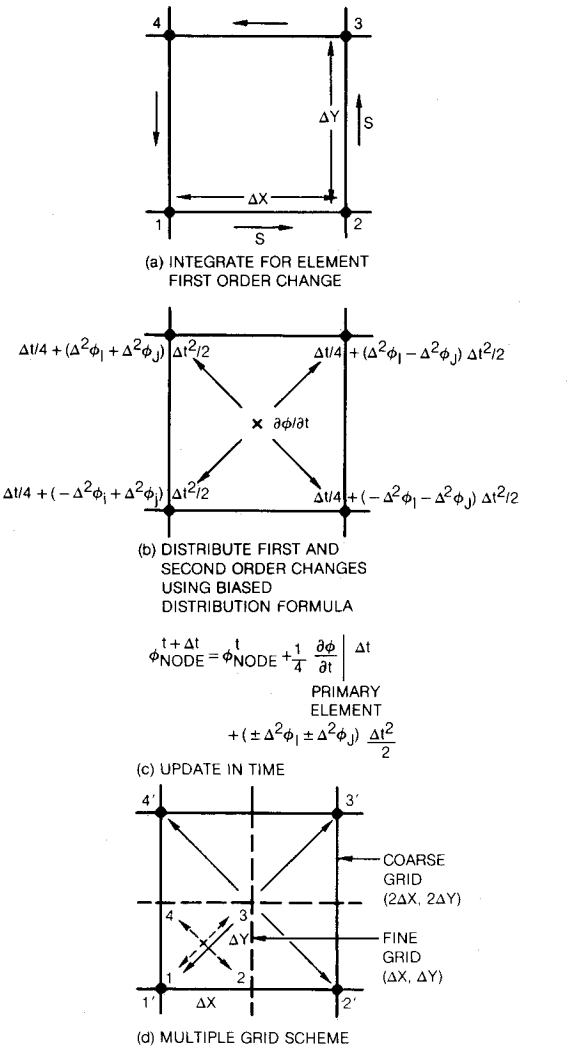

Fig. 4 Control volume one-step technique.

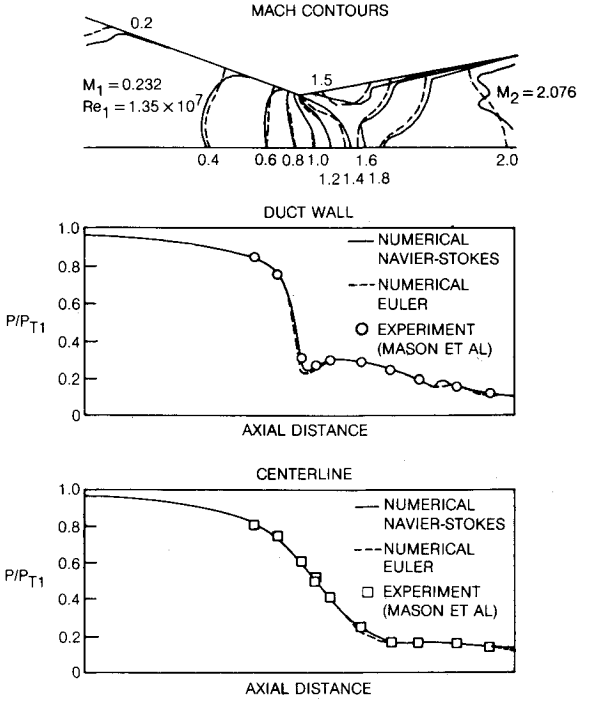

Fig. 5 Comparison of finite element two-step technique with experimental data for the Mason B1 nozzle.

primary variables in time according to the flow equations. Since a distribution of time-rate changes only occurs from the computational domain, the radiation condition assumes that the flow outside of the computational domain is at equilibrium or steady state. Waves of time-rate primary variable change, therefore, are not produced from the exterior region. Convergence of the numerical scheme to a steady-state solution is enhanced through the use of this boundary condition.

For solid boundaries, a "no-slip" condition for viscous flow and a "slip" condition for inviscid flow are imposed at the wall. The first- and second-order changes in time of the velocity components are set to zero for viscous flow in accordance with the no-slip condition. A wave reflection condition, where the changes in the primary variables are doubled at the wall, is used for the velocity components in inviscid flow and for the density in both inviscid and viscous flows. Both the first- and second-order changes in time of the primary variables at the solid boundaries are typically only one-half of those at the interior nodes. The wave reflection condition is used to correct these differences and model the actual wave phenomena at the wall.

In the calculation of the second-order changes along the boundaries for the finite element two-step technique, imaginary nodes a distance of one-half primary element length away from the boundaries are used, as shown in Fig. 3. The values of the first-order changes in time at these imaginary nodes are assumed to be zero.

Smoothing—Artificial Viscosity

As has been shown by Ni and others, it becomes apparent that artificial viscosity in the form of numerical smoothing of primary variables must be introduced to the time-marching scheme in order to maintain stability in supersonic, high Reynolds number flows. Smoothing of the type discussed by Ni is used in this computational technique. This smoothing enables the scheme to converge to the correct physical solution in regions where shocks exist but does tend to flatten the gradients in pressure over two elements. Laminar shear stresses do not produce enough physical viscous smoothing in these flows to stabilize the scheme necessitating numerical smoothing. The numerical smoothing is kept at minimum levels, though. Smoothing of the density has been found to be useful in low-speed freestream flows ($M \leq 0.1$), as well as to enhance convergence which is slowed due to low wave speeds and the corresponding small time steps.

Control Volume One-Step Technique

The control volume one-step technique consists of calculating the first-order change in time of the primary variables ρ, ρu, and ρv by integrating Eqs. (1-3) using a simple flux summing scheme. A biased distribution of element first-order changes is given to each corner node of the primary element. This distribution consists of $1/N$ plus an area-weighted portion of the element change to each corner node. The area-weighted portion is biased positive or negative such that the net effect of the distribution of changes from elements surrounding a given node results in the calculation of the second-order time-rate change at the node. Time-step and boundary condition requirements are the same as for the finite element two-step technique.

First-Order Changes in Time

The control volume one-step scheme may be shown to be a subset of the finite element two-step technique. First-order changes in time are calculated similar to the finite element two-step technique by integrating Eqs. (1-3) over small polygons but using a projected area technique instead of finite elements. By choosing bilinear elements and linear primary variable functions within the element, a simple trapezoidal integration procedure arises. This procedure consists of

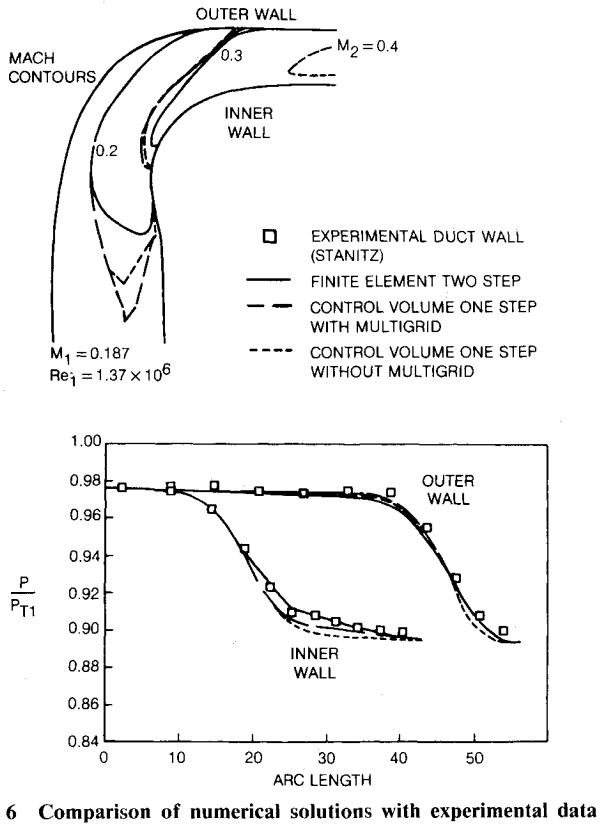

Fig. 6 Comparison of numerical solutions with experimental data for the Stanitz duct.

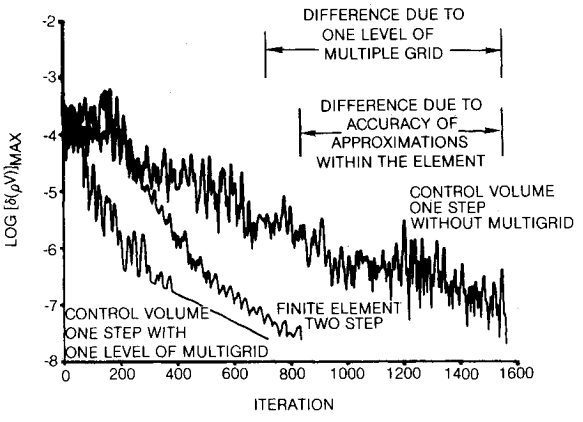

Fig. 7 Comparison of convergence rates of finite element and control volume techniques.

taking the average flux on the face of a control volume and multiplying it by the area projected perpendicular to the x or y directions to obtain the mass or momentum traveling across that face in those directions. A proper summing of the mass and momentum of the faces around the control volume results in an integration of the Navier-Stokes equations and the first-order change in time of the primary variables.

Consider the simple case of the integration of ϕ over a two-dimensional unit square element, as shown in Fig. 1a. Let ϕ be represented in each of the subvolumes of the element by a function such as that of Eq. (9). For subvolume 1, Eq. (9) becomes

$$\phi_e = [1 \; x \; y] \begin{bmatrix} 1 & 0 & 0 \\ -1 & 1 & 0 \\ -1 & 0 & 1 \end{bmatrix} [\phi_i] \tag{15}$$

Since $[\phi_i]$ and the stiffness matrix are constant over the subvolume, the integration of Eq. (15) involves only the shape function, $[SF]$. For example, the closed integral of ϕ with respect to x is

$$\oint_{\text{s.v.1}} \phi_e dx = [0.5 \;\; 0 \;\; -0.5][\phi_i] \tag{16}$$

The same process may be carried out for subvolume 2 of Fig. 1a to give

$$\oint_{\text{s.v.2}} \phi_e dx = [-0.5 \;\; 0 \;\; 0.5][\phi_i] \tag{17}$$

The closed integral around the total element may be performed by assembling the matrices on the right-hand side of Eqs. (16) and (17). This is performed in the following manner:

$$\begin{array}{l}\text{node:}\quad 1\;\;2\quad\;\; 4\qquad\quad 3\;\;4\;\;2\qquad 1\;\;2\qquad 3\qquad 4\\ [0.5\;0\;-0.5]+[-0.5\;0\;0.5]=[0.5\;0.5\;-0.5\;\;-0.5]\end{array} \tag{18}$$

so that

$$\oint_{\text{polygon}} \phi_e dx = [0.5 \;\; 0.5 \;\; -0.5 \;\; -0.5][\phi_i] \tag{19}$$

Equation (19) is simply the sum of the average ϕ of each face of the element multiplied by the corresponding change in x across that face. In the same fashion, a closed integral of a function with respect to y may be performed by multiplying the average value of the function along each face of the control volume by its corresponding change in y and summing the results. Appendix B gives the control volume equations for the calculation of the first-order changes in time using this technique with the Navier-Stokes equations. The calculation of all shear stress terms within the control volume one-step scheme remains the same as that of the finite element technique. Figure 4a demonstrates the first-order change calculation step.

Second-Order Changes in Time

Since integrations may be performed through summing of area-weighted face fluxes, the second-order change integration may be included in the distribution step. By adding or subtracting area-weighted first-order element change fluxes to the nodes as part of the distribution step, an integration of the second-order change equations is performed. This step is shown in Fig. 4b. Ni was the first to use this technique for the solution of the Euler equations. Appendix B gives the resulting distribution equations for the control volume one-step scheme. Unsteady shear stress terms associated with the time derivative of the Navier-Stokes equations are usually ignored in this scheme, as is done in the finite element technique.

Multiple-Grid Scheme

Since the unsteady shear stresses usually may be neglected, the Ni multiple-grid convergence acceleration scheme may be used to reach steady-state solutions in considerably fewer time-step iterations. This multiple-grid scheme takes the total of the first- and second-order changes that exist at the nodes from the fine grid, interprets them as element first-order changes of a grid that has been doubled in size, distributes $1/N$ of the new element changes plus the biased second-order changes to the corner nodes of the larger primary elements, interpolates the new changes at intermediate nodes, and updates the primary variables. This process continues on successively larger grids. Figure 4d demonstrates this step in the control volume scheme.

Results and Discussion

The described finite element and control volume numerical techniques have been tested on a variety of viscous flow problems. The results of three cases demonstrates that the present schemes are stable and accurate over a wide range of flow conditions.

Supersonic Nozzle

Figure 5 shows the comparison of the finite element viscous solution with experimental data for a planar nozzle (B1) reported by Mason et al.[9] The experimental data were taken at midspan of the duct walls and on the centerline of the endwalls. By dropping the viscous terms ($\mu = 0.0$) in the basic solver, the solution to the Euler equations also may be obtained using the same technique. Excellent agreement between the numerical solutions and the experimental data exists for both the nozzle wall and centerline positions. A 49×6 point uniform mesh breakup was used in the Euler solution of the half-nozzle, whereas a 49×13 point mesh was used in the Navier-Stokes solution. The streamwise mesh lines were spaced quadratically from the nozzle wall to the centerline in the Navier-Stokes mesh. The Euler and Navier-Stokes solutions took 270 and 570 time steps, respectively, to reach convergence. Convergence was reached when the maximum change in the total flux at every node was less than 0.0005.

The three-dimensional Euler solution was predicted for this nozzle using a $49 \times 6 \times 6$ uniformly spaced computational mesh. The resulting pressure distribution of this calculation is identical to that of the two-dimensional Euler solution. The calculation took 740 time steps to reach steady state.

Turning Duct

Figure 6 shows the results of the finite element numerical scheme with experimental data for a 90-deg turning duct reported by Stanitz et al.[10] The experimental data located at midspan of the duct were taken at a 0.4 exit Mach number with "clean" (no spoiler) inlet flow. A 47×21 point mesh was used in the Navier-Stokes solution where the mesh was spaced quadratically away from the wall. At least two computational points were defined inside of the viscous boundary-layer region adjacent to each duct wall. The solution took 840 time steps to reach steady state.

The three-dimensional finite element code was run on the Stanitz duct at the same aerodynamic conditions. An Euler solution was calculated on a $49 \times 9 \times 4$ uniform mesh for the half-duct taking 870 iterations to reach convergence. As expected, the inviscid pressure distribution is identical to the two-dimensional Euler and Navier-Stokes solutions since the endwalls of the duct are planar. A preliminary prediction of the Navier-Stokes solution was made using a $50 \times 15 \times 8$ mesh. The mesh was spaced quadratically from each wall for the half-duct geometry. A steady-state solution was reached in 1340 iterations. Barber[11] and Moore and Moore[12,13] have modeled the flow in this duct successfully for the case when inlet boundary layers where increased in size with spoilers thus amplifying the secondary flow and reducing the need for very fine mesh spacing. It has been found that in order to predict the exit plane stagnation pressure loss contours accurately for the clean inlet boundary-layer case, the mesh density needed to resolve the flow structure must be much greater than that used in this initial attempt. The computational times required to calculate three-dimensional flows with greater mesh densities using the finite element two-step code are unacceptable, however, until the multiple-grid accelerator can be connected.

The results of the control volume one-step technique for the Stanitz duct with and without the multiple-grid effects are also shown in Fig. 6 using the same mesh as used in the two-dimensional finite element calculations. One level of the

multiple-grid scheme was used for this grid. Differences in the locations of the Mach number contour locations of the finite element and control volume schemes are attributed to the difference in the accuracy of the approximations used within the elements of the two techniques. The use of basis functions for the density and velocity components in the finite element scheme, as compared to the linear approximations used for the density and mass flux components in the control volume scheme, results in a more accurate representation of the Navier-Stokes equations. Figure 7 demonstrates the convergence history for the cases shown in Fig. 6. The accuracy of the finite element technique results in a lower number of time steps to reach convergence than the basic control volume scheme (without multiple-grid). The amount of extra computing time involved in attaining the higher accuracy, though, leads to greater computational times for the finite element scheme. The basic control volume scheme took 1560 iterations to reach steady state. The control volume scheme with the use of the multiple-grid routine took 720 time steps to reach convergence. The use of the multiple-grid acceleration routine demonstrates a significant savings in both time steps and computational time compared to the finite element technique and the basic control volume scheme.

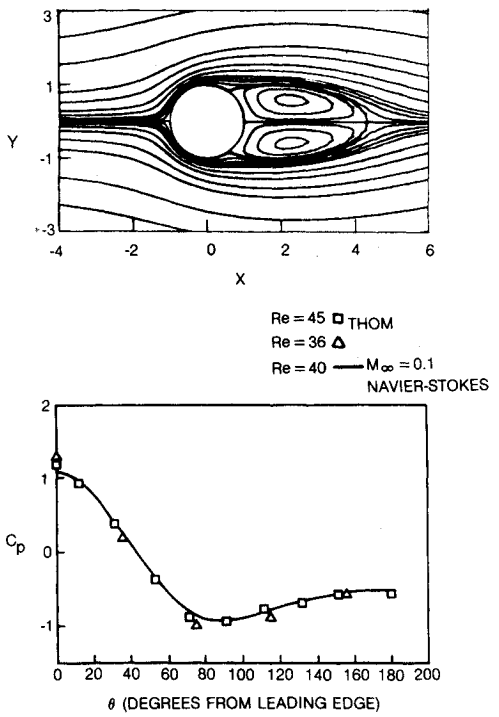

Fig. 8 Comparison of control volume one-step technique with experimental data.

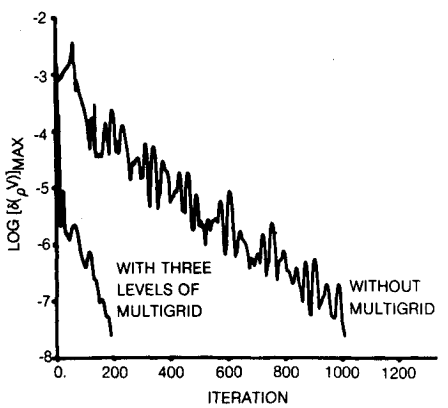

Fig. 9 Comparison of convergence rates of control volume one-step technique with and without multiple-grid.

Cylinder

Computational efficiency and accuracy for the control volume one-step technique is demonstrated in Fig. 8 for the case of flow over an isolated cylinder. The freestream Mach number is 0.1 and the Reynolds number based upon cylinder diameter is 40. A 129×33 point polar grid was used for the calculations shown in Figs. 8 and 9. The mesh was spaced quadratically from the surface. Along the freestream boundary, located 3.5 diameters from the cylinder surface, the total pressure was held constant at all inflow boundary points and a radiation condition was used at the outflow points. The predicted surface pressure distribution of the control volume scheme is compared with experimental data taken by Thom.[14] These results, along with the calculated streamline pattern shown, demonstrate the ability of this code to predict viscous dominated flows efficiently using the multiple-grid scheme.

The convergence rates of the control volume scheme with and without the multiple-grid acceleration routine are shown in Fig. 9. The basic scheme (without multiple-grid) took 1010 iterations and 970 s on an IBM 3081 computer to reach a steady-state solution. The same scheme run with three levels of the multiple-grid technique took 190 iterations and 230 s to converge. An 81% savings in time steps and a 77% savings in computational time is realized for this case with the utilization of the multiple-grid scheme.

Conclusions

This paper presents a new technique for solving the laminar Navier-Stokes equations using an explicit, second-order accurate, control volume, time-marching routine. A two-step control volume scheme which utilizes finite elements in the integration steps of the numerical approach is defined and described. As a subset to this scheme, a one-step control volume routine, which uses a formula to distribute biased time-rate changes from control volumes to the grid points, has been developed also. The new technique has been combined with the Ni multiple-grid convergence acceleration algorithm to calculate laminar viscous flow efficiently. Time-step and boundary condition requirements for this technique are described.

Cases of internal and external laminar flows demonstrate that the technique is stable and accurate for a wide range of conditions, including supersonic and viscous dominated flows. The finite element two-step technique has two basic advantages over the control volume one-step scheme. The finite element solver has more accurate approximations within each element and has a faster convergence rate than the basic control volume scheme. However, the finite element solver requires more computational time than the control volume scheme due to the element approximations and the two-step algorithm. The control volume one-step scheme has the main advantage of efficiency over the finite element scheme. The use of the multiple-grid acceleration routine may be used with either approach to greatly reduce the computational time to obtain steady-state viscous solutions.

Appendix A: Finite Element First-Order Change Equations

Continuity:

$$\frac{A}{\Delta t}\Delta\rho = -[\rho_i]^*[\mathrm{ISF2Y}][u_i] + [\rho_i]^*[\mathrm{ISF2X}][v_i] \qquad \text{(A1)}$$

Axial momentum:

$$\frac{A}{\Delta t}\Delta\rho u = -RT_T[\mathrm{ISFY}][\rho_i] + [\rho u_i]^*[\mathrm{ISF2X}][v_i] - \frac{\gamma+1}{2\gamma}[\rho u_i]^*[\mathrm{ISF2Y}][u_i] + \frac{\gamma-1}{2\gamma}[\rho v_i]^*[\mathrm{ISF2Y}][v_i] + \mu\left[\frac{4}{3}[\mathrm{ISFY}]\left[\frac{\partial u}{\partial x}i\right] - \frac{2}{3}[\mathrm{ISFY}]\left[\frac{\partial v}{\partial y}i\right] - [\mathrm{ISFX}]\left[\frac{\partial u}{\partial y}i\right] - [\mathrm{ISFX}]\left[\frac{\partial v}{\partial x}i\right]\right] \quad \text{(A2)}$$

Tangential momentum:

$$\frac{A}{\Delta t}\Delta\rho v = RT_T[\mathrm{ISFX}][\rho_i] - [\rho u_i]^*[\mathrm{ISF2Y}][v_i] + \frac{\gamma+1}{2\gamma}[\rho v_i]^*[\mathrm{ISF2X}][v_i] - \frac{\gamma-1}{2\gamma}[\rho u_i]^*[\mathrm{ISF2X}][u_i] + \mu\left[-\frac{4}{3}[\mathrm{ISFX}]\left[\frac{\partial v}{\partial y}i\right] + \frac{2}{3}[\mathrm{ISFX}]\left[\frac{\partial u}{\partial x}i\right] + [\mathrm{ISFY}]\left[\frac{\partial u}{\partial y}i\right] + [\mathrm{ISFY}]\left[\frac{\partial v}{\partial x}i\right]\right] \quad \text{(A3)}$$

where

$$[\mathrm{ISF2Y}] = [K]^* \oint [\mathrm{SF2}]\mathrm{d}y[K]$$

$$[\mathrm{ISF2X}] = [K]^* \oint [\mathrm{SF2}]\mathrm{d}x[K]$$

$$[\mathrm{ISFY}] = \oint [\mathrm{SF}]^*\mathrm{d}y[K]$$

$$[\mathrm{ISFX}] = \oint [\mathrm{SF}]^*\mathrm{d}x[K]$$

$$[\mathrm{SF2}] = [\mathrm{SF}][\mathrm{SF}]^* \quad \text{(A4)}$$

Appendix B: Control Volume One-Step Equations

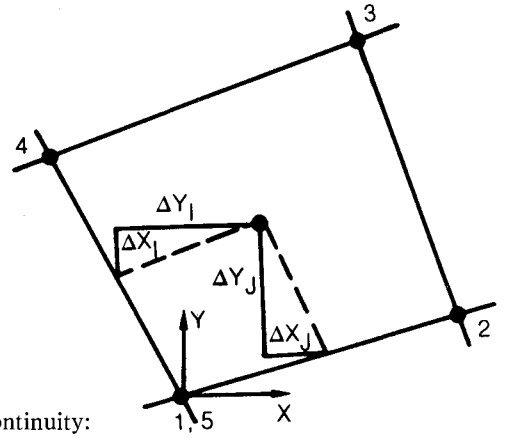

Continuity:

$$\frac{A}{\Delta t}\Delta\rho = \sum_{k=1}^{4} -\frac{1}{2}(\rho u_k + \rho u_{k+1})\Delta y_k + \frac{1}{2}(\rho v_k + \rho v_{k+1})\Delta x_k \quad \text{(B1)}$$

Axial momentum:

$$\frac{A}{\Delta t}\Delta\rho u = \sum_{k=1}^{4} -\frac{1}{2}(\rho u_k^2 + \rho u_{k+1}^2)\Delta y_k - \frac{1}{2}(p_k + p_{k+1})\Delta y_k + \frac{1}{2}(\rho uv_k + \rho uv_{k+1})\Delta x_k + \mu\left[\frac{2}{3}\left[\frac{\partial u}{\partial x}k + \frac{\partial u}{\partial x}k+1\right]\Delta y_k - \frac{1}{3}\left[\frac{\partial v}{\partial y}k + \frac{\partial v}{\partial y}k+1\right]\Delta y_k - \frac{1}{2}\left[\frac{\partial u}{\partial y}k + \frac{\partial u}{\partial y}k+1\right]\Delta x_k - \frac{1}{2}\left[\frac{\partial v}{\partial x}k + \frac{\partial v}{\partial x}k+1\right]\Delta x_k\right] \quad \text{(B2)}$$

Tangential momentum:

$$\frac{A}{\Delta t}\Delta\rho v = \sum_{k=1}^{4} \frac{1}{2}(\rho v_k^2 + \rho v_{k+1}^2)\Delta x_k + \frac{1}{2}(p_k + p_{k+1})\Delta x_k - \frac{1}{2}(\rho uv_k + \rho uv_{k+1})\Delta y_k + \mu\left[-\frac{2}{3}\left[\frac{\partial v}{\partial y}k + \frac{\partial v}{\partial y}k+1\right]\Delta x_k + \frac{1}{3}\left[\frac{\partial u}{\partial x}k + \frac{\partial u}{\partial x}k+1\right]\Delta x_k + \frac{1}{2}\left[\frac{\partial u}{\partial y}k + \frac{\partial u}{\partial y}k+1\right]\Delta y_k + \frac{1}{2}\left[\frac{\partial v}{\partial x}k + \frac{\partial v}{\partial x}k+1\right]\Delta y_k\right] \quad \text{(B3)}$$

where

$$\Delta x_k = x_{k+1} - x_k \quad \Delta y_k = y_{k+1} - y_k$$

$$A = \tfrac{1}{2}[(x_3 - x_1)(y_4 - y_2) - (x_4 - x_2)(y_3 - y_1)]$$

$$\Delta x_I = \tfrac{1}{4}(x_2 + x_3 - x_1 - x_4) \quad \Delta x_J = \tfrac{1}{4}(x_3 + x_4 - x_1 - x_2)$$

$$\Delta y_I = \tfrac{1}{4}(y_2 + y_3 - y_1 - y_4) \quad \Delta y_J = \tfrac{1}{4}(y_3 + y_4 - y_1 - y_2) \quad \text{(B4)}$$

and

$$\phi_1^{t+\Delta t} = \phi_1^t + \tfrac{1}{4}\Delta\phi - \tfrac{1}{2}\Delta^2\phi_I + \tfrac{1}{2}\Delta^2\phi_J$$

$$\phi_2^{t+\Delta t} = \phi_2^t + \tfrac{1}{4}\Delta\phi - \tfrac{1}{2}\Delta^2\phi_I - \tfrac{1}{2}\Delta^2\phi_J$$

$$\phi_3^{t+\Delta t} = \phi_3^t + \tfrac{1}{4}\Delta\phi + \tfrac{1}{2}\Delta^2\phi_I - \tfrac{1}{2}\Delta^2\phi_J$$

$$\phi_4^{t+\Delta t} = \phi_4^t + \tfrac{1}{4}\Delta\phi + \tfrac{1}{2}\Delta^2\phi_I + \tfrac{1}{2}\Delta^2\phi_J$$

$$\phi = \rho,\ \rho u,\ \rho v \quad \text{(B5)}$$

$$\frac{A}{\Delta t^2}\Delta^2\rho_I = -\frac{\partial\rho u}{\partial t}\Delta y_I + \frac{\partial\rho v}{\partial t}\Delta x_I$$

$$\frac{A}{\Delta t^2}\Delta^2\rho_J = -\frac{\partial\rho u}{\partial t}\Delta y_J + \frac{\partial\rho v}{\partial t}\Delta x_J \quad \text{(B6)}$$

$$\frac{A}{\Delta t^2}\Delta^2\rho u_I = -\frac{\partial\rho u^2}{\partial t}\Delta y_I - \frac{\partial p}{\partial t}\Delta y_I + \frac{\partial\rho uv}{\partial t}\Delta x_I$$

$$\frac{A}{\Delta t^2}\Delta^2\rho u_J = -\frac{\partial\rho u^2}{\partial t}\Delta y_J - \frac{\partial p}{\partial t}\Delta y_J + \frac{\partial\rho uv}{\partial t}\Delta x_J \quad \text{(B7)}$$

$$\frac{A}{\Delta t^2}\Delta^2 \rho v_I = \frac{\partial \rho v^2}{\partial t}\Delta x_I + \frac{\partial p}{\partial t}\Delta x_I - \frac{\partial \rho uv}{\partial t}\Delta y_I$$

$$\frac{A}{\Delta t^2}\Delta^2 \rho v_J = \frac{\partial \rho v^2}{\partial t}\Delta x_J + \frac{\partial p}{\partial t}\Delta x_J - \frac{\partial \rho uv}{\partial t}\Delta y_J \qquad \text{(B8)}$$

Acknowledgments

The first author wishes to thank J. F. Dannenhoffer, J. R. Caspar, and T. J. Barber of the United Technologies Corporation for their encouragement, guidance, and helpful discussions. The research presented in this paper was funded by the University of Connecticut Graduate School and Pratt and Whitney Aircraft. The authors wish to thank the managers of each for their financial support in this project. Part of the work reported herein was performed while the first author was on a leave of absence in the University of Connecticut Ph.D. Program.

References

[1] Spradley, L. W., Stalnaker, J. T., and Ratliff, A. W., "Computation of Three Dimensional Viscous Flows with the Navier-Stokes Equations," AIAA Paper 80-1348, July 1980.

[2] MacCormack, R. W., "The Effect of Viscosity in Hypervelocity Impact Cratering," AIAA Paper 69-345, May 1969.

[3] MacCormack, R. W., "A Numerical Method for Solving the Equations of Compressible Viscous Flow," AIAA Paper 81-0110, Jan. 1981.

[4] Ni, R. H., "A Multiple Grid Scheme for Solving the Euler Equations," *AIAA Journal*, Vol. 20, Nov. 1982, pp. 1565-1571.

[5] Johnson, G. M., "Convergence Acceleration of Viscous Flow Computations," NASA TM-83039, 1982.

[6] Davis, R. L., "The Prediction of Compressible, Viscous Secondary Flow in Channel Passages," Ph.D. Dissertation, University of Connecticut, Storrs, Conn., July 1982.

[7] Courant, R. , Friedricks, K. O., and Lewy, H., "Uber die Partiellen Differenzengleichungen der Mathematischen," *Physik. Math. Ann.*, Vol. 100, 1928, p. 32.

[8] Richtmyer, R. D. and Morton, K. W., *Difference Methods for Initial Value Problems*, Wiley and Sons, New York, 1967.

[9] Mason, M. L., Putnam, L. E., and Re, R. J., "The Effect of Throat Contouring on Two-Dimensional Converging-Diverging Nozzles at Static Conditions," NASA TP 1704, Aug. 1980.

[10] Stanitz, J. D., Osborn, W. M., and Mizisin, J., "An Experimental Investigation of Secondary Flow in Accelerating Rectangular Elbow with 90 of Turning," NACA TN 3015.

[11] Barber, T. J., "Analysis of Shearing Internal Flows," AIAA Paper 81-0005, 1981.

[12] Moore, J. and Moore, J. G., "A Calculation Procedure for 3-D Viscous Compressible Duct Flows," *Journal of Fluids Engineering*, Vol. 101, Dec. 1979, pp. 415-422.

[13] Moore, J. and Moore, J. G., "Three-Dimensional Flow and Stagnation Pressure Losses in an Accelerating Rectangular Elbow with 90 Degrees of Turning," *Journal of Fluids Engineering*, Vol. 101, Dec. 1979, pp. 423-428.

[14] Thom, A., "The Flows Past Circular Cylinders at Low Speeds," *Proceedings of the Royal Society of London*, Series A, Vol. 141, 1933, p. 651.